3.3 Nonlinear Raman Spectroscopy

When the intensity of the incident light wave becomes sufficiently large, the induced oscillation of the electron cloud surpasses the linear range assumed in Sect. 3.1. This implies that the induced dipole moments p of the molecules are no longer proportional to the electric field $\boldsymbol{E}$ and we have to generalize (3.2). The function $\boldsymbol{p}(\boldsymbol{E})$ can be expanded into a power series of E^n $(n = 0, 1, 2, \dots)$, which is generally written as

$$\boldsymbol{p}(\boldsymbol{E}) = \boldsymbol{\mu} + \tilde{\alpha}\boldsymbol{E} + \tilde{\beta}\boldsymbol{E}\cdot\boldsymbol{E} + \tilde{\gamma}\boldsymbol{E}\cdot\boldsymbol{E}\cdot\boldsymbol{E}\,, \tag{3.18a}$$

where $\tilde{\alpha}$ is the polarizability tensor, $\tilde{\beta}$ is named *hyper-polarizability*, and $\tilde{\gamma}$ is called the *second hyper-polarizability*. The quantities α, β, and γ are tensors of rank two, three, and four, respectively.

In component notation $(i = x, y, z)$ (3.18a) can be written as

$$p_i(\boldsymbol{E}) = \mu_i + \sum_k \alpha_{ik}E_k + \sum_k\sum_j \beta_{ikj}E_kE_j + \sum_k\sum_j\sum_l \gamma_{ikjl}E_kE_jE_l\,. \tag{3.18b}$$

This gives for the polarization $\boldsymbol{P} = N\boldsymbol{p}$ of a medium with N oriented dipoles

$$P_i(\boldsymbol{E}) = \epsilon_0\left(\chi_i + \sum_k \chi_{ik}E_k + \sum_{k,j}\chi_{ikj}E_kE_j + \dots\right)\,, \tag{3.18c}$$

which corresponds to Vol. 1, (5.114) discussed in the section on nonlinear optics and frequency conversion, if we define the susceptibilities $\chi_i = N\mu_i/\epsilon_0$, $\chi_{ik} = N\alpha_{ik}/\epsilon_0$, and so on.

For sufficiently small electric field amplitudes E the nonlinear terms in (3.18a) can be neglected, and we then obtain (3.2) for the linear Raman spectroscopy.

3.3.1 Stimulated Raman Scattering

If the incident laser intensity I_L becomes very large, an appreciable fraction of the molecules in the initial state E_i is excited into the final state E_f and the intensity of the Raman-scattered light is correspondingly large. Under these conditions we have to consider the simultaneous interaction of the molecules with *two* EM waves: the laser wave at the frequency ω_L and the Stokes wave at the frequency $\omega_\mathrm{S} = \omega_\mathrm{L} - \omega_\mathrm{V}$ or the anti-Stokes wave at $\omega_\mathrm{a} = \omega_\mathrm{L} + \omega_\mathrm{V}$. Both waves are coupled by the molecules vibrating with the frequencies ω_V. This parametric interaction leads to an energy exchange between the pump wave and the Stokes or anti-Stokes waves. This phenomenon of *stimulated* Raman scattering, which was first observed by Woodbury et al. [3.39] and then explained by Woodbury and Eckhardt [3.40], can be described in classical terms [3.41, 3.42].

The Raman medium is taken as consisting of N harmonic oscillators per unit volume, which are independent of each other. Because of the combined action of the incident laser wave and the Stokes wave, the oscillators experience a driving force $\boldsymbol{F}$ that depends on the total field amplitude $\boldsymbol{E}$

$$\boldsymbol{E}(z,t) = \boldsymbol{E}_{\mathrm{L}} \mathrm{e}^{\mathrm{i}(\omega_{\mathrm{L}} t - k_{\mathrm{L}} z)} + \boldsymbol{E}_{\mathrm{S}} \mathrm{e}^{\mathrm{i}(\omega_{\mathrm{S}} t - k_{\mathrm{S}} z)} , \tag{3.19}$$

where we have assumed plane waves traveling in the z-direction. The potential energy W_{pot} of a molecule with induced dipole moment $\boldsymbol{p} = \alpha \boldsymbol{E}$ in an EM field with amplitude $\boldsymbol{E}$ is, according to (3.2, 3.3) with $\mu = 0$

$$W_{\mathrm{pot}} = -\boldsymbol{p} \cdot \boldsymbol{E} = -\alpha(q) E^2 . \tag{3.20}$$

The force $\boldsymbol{F} = -\mathrm{grad}\, W_{\mathrm{pot}}$ acting on the molecule gives

$$\boldsymbol{F}(z,t) = +\frac{\partial}{\partial q}\{[\alpha(q)]E^2\} = \left(\frac{\partial \alpha}{\partial q}\right)_0 E^2(z,t) . \tag{3.21}$$

The equation of motion for the molecular oscillator with oscillation amplitude q, mass m, and vibrational eigenfrequency ω_{v} is then

$$\frac{\partial^2 q}{\partial t^2} - \gamma \frac{\partial q}{\partial t} + \omega_{\mathrm{v}}^2 q = \left(\frac{\partial \alpha}{\partial q}\right)_0 E^2/m , \tag{3.22}$$

where γ is the damping constant that is responsible for the linewidth $\Delta\omega = \gamma$ of spontaneous Raman scattering. Inserting the complex ansatz

$$q = \frac{1}{2}\left(q_{\mathrm{v}} \mathrm{e}^{\mathrm{i}\omega t} + q_{\mathrm{v}}^* \mathrm{e}^{-\mathrm{i}\omega t}\right) , \tag{3.23}$$

into (3.22) we get with the field amplitude (3.19)

$$(\omega_{\mathrm{v}}^2 - \omega^2 + \mathrm{i}\gamma\omega) q_{\mathrm{v}} \mathrm{e}^{\mathrm{i}\omega t} = \frac{1}{2m}\left(\frac{\partial \alpha}{\partial q}\right)_0 E_{\mathrm{L}} E_{\mathrm{S}} \mathrm{e}^{\mathrm{i}[(\omega_{\mathrm{L}} - \omega_{\mathrm{S}})t - (k_{\mathrm{L}} - k_{\mathrm{S}})z]} . \tag{3.24}$$

Comparison of the time-dependent terms on both sides of (3.24) shows that $\omega = \omega_{\mathrm{L}} - \omega_{\mathrm{S}}$. The molecular vibrations are therefore driven at the difference frequency $\omega_{\mathrm{v}} = \omega_{\mathrm{L}} - \omega_{\mathrm{S}}$. Solving (3.24) for q_{v} yields

$$q_{\mathrm{v}} = \frac{(\partial \alpha/\partial q)_0 E_{\mathrm{L}} E_{\mathrm{S}}}{2m[\omega_{\mathrm{v}}^2 - (\omega_{\mathrm{L}} - \omega_{\mathrm{S}})^2 + \mathrm{i}(\omega_{\mathrm{L}} - \omega_{\mathrm{S}})\gamma]} \mathrm{e}^{-\mathrm{i}(k_{\mathrm{L}} - k_{\mathrm{S}})z} . \tag{3.25}$$

The induced oscillating molecular dipoles $\boldsymbol{p}(\omega, z, t)$ result in a macroscopic polarization $P = Np$. According to (3.5), the polarization $P_{\mathrm{S}} = P(\omega_{\mathrm{S}})$ at the Stokes frequency ω_{S}, which is responsible for Raman scattering, is given by

$$P_{\mathrm{S}} = \frac{1}{2} N \left(\frac{\partial \alpha}{\partial q}\right)_0 qE . \tag{3.26}$$

Inserting q from (3.23, 3.25) and E from (3.19) yields the *nonlinear* polarization

$$P_S^{NL}(\omega_S) = N\frac{(\partial\alpha/\partial q)_0^2 E_L^2 E_S}{4m[\omega_v^2 - (\omega_L - \omega_S)^2 + i\gamma(\omega_L - \omega_S)]} e^{-i(\omega_s t - k_s z)} . \quad (3.27)$$

This shows that a *polarization wave* travels through the medium with an amplitude proportional to the product $E_L^2 \cdot E_S$. It has the same wave vector k_S as the Stokes wave and can therefore amplify this wave. The amplification can be derived from the wave equation

$$\Delta E = \mu_0\sigma\frac{\partial}{\partial t}E + \mu_0\epsilon\frac{\partial^2}{\partial t^2}E + \mu_0\frac{\partial^2}{\partial t^2}\left(P_S^{NL}\right) , \quad (3.28)$$

for waves in a medium with the conductivity σ, where P_S^{NL} acts as the driving term.

For the one-dimensional problem ($\partial/\partial y = \partial/\partial x = 0$) with the approximation $d^2E/dz^2 \ll k\,dE/dz$ and with (3.26), the equation for the Stokes wave becomes

$$\frac{dE_S}{dz} = -\frac{\sigma}{2}\sqrt{\mu_0/\epsilon}E_S + N\frac{k_S}{2\epsilon}\left(\frac{\partial\alpha}{\partial q}\right)_0 q_v E_L . \quad (3.29)$$

Substituting q_v from (3.25) gives the final result for the case $\omega_v = \omega_L - \omega_S$

$$\frac{dE_S}{dz} = \left[-\frac{\sigma}{2}\sqrt{\mu_0/\epsilon} + N\frac{(\partial\alpha/\partial q)_0^2 E_L^2}{4m\epsilon i\gamma(\omega_L - \omega_S)}\right] E_S = (-f + g)E_S . \quad (3.30)$$

Integration of (3.30) yields

$$E_S = E_S(0)\,e^{(g-f)z} . \quad (3.31a)$$

The Stokes wave is amplified if the gain g exceeds the losses f. The amplification factor g depends on the square of the laser amplitude E_L and on the term $(\partial\alpha/\partial q)_0^2$. Stimulated Raman scattering is therefore observed only if the incident laser intensity exceeds a threshold value that is determined by the nonlinear term $(\partial\alpha_{ij}/\partial q)_0$ in the polarization tensor of the Raman-active normal vibration and by the loss factor $f = \frac{1}{2}\sigma(\mu_0/\epsilon)^{1/2}$.

According to (3.31), the Stokes intensity increases exponentially with the length z of the interaction zone. If, however, the pump wave is absorbed by the medium, the pump intensity at the position z decreases to

$$I_L(z) = I_L(0) \cdot e^{-\alpha \cdot z}$$

and therefore the gain factor g in (3.30) is smaller. There is an effective length $z = L_{eff}$ for the optimum intensity I_s of the Stokes wave, which is given by

$$L_{eff} = (1/\alpha_L)[1 - e^{-\alpha \cdot L}]$$

and the amplitude of the Stokes wave becomes for a medium with length L

$$E_s = E_s(0) \cdot e^{(g \cdot L_{eff} - f \cdot L)} . \tag{3.31b}$$

While the intensity of anti-Stokes radiation is very small in spontaneous Raman scattering due to the low thermal population density in excited molecular levels (Sect. 3.1), this is not necessarily true in stimulated Raman scattering. Because of the strong incident pump wave, a large fraction of all interacting molecules is excited into higher vibrational levels, and strong anti-Stokes radiation at frequencies $\omega_L + \omega_v$ has been found.

According to (3.26), the driving term in the wave equation (3.28) for an anti-Stokes wave at $\omega_a = \omega_L + \omega_V$ is given by

$$P^{NL}_{\omega_a} = \frac{1}{2} N \left(\frac{\partial \alpha}{\partial q} \right)_0 q_v E_L \, e^{i[(\omega_L + \omega_v)t - k_L z]} , \tag{3.32}$$

For small amplitudes $E_a \ll E_L$ of the anti-Stokes waves, we can assume that the molecular vibrations are independent of E_a and can replace q_v by its solution (3.25). This yields an equation for the amplification of E_a that is analogous to (3.29) for E_S

$$\frac{dE_a}{dz} = -\frac{f}{2} E_a \, e^{i(\omega_a t - k_a z)} + N_v \left[\frac{\omega_a \sqrt{\mu_0/\epsilon}}{8 m_v} \left(\frac{\partial \alpha}{\partial q} \right)^2_0 \right] E_L^2 E_S^* \, e^{i(2k_L - k_S - k_a)z} , \tag{3.33}$$

where N_v is the density of vibrationally excited molecules. This shows that, analogously to sum- or difference-frequency generation (Vol. 1, Sect. 5.8), a macroscopic wave can build up only if the phase-matching condition

$$k_a = 2k_L - k_S , \tag{3.34}$$

can be satisfied. In a medium with normal dispersion this condition cannot be met for collinear waves. From a three-dimensional analysis, however, one obtains the vector equation

$$2\boldsymbol{k}_L = \boldsymbol{k}_S + \boldsymbol{k}_a , \tag{3.35}$$

which reveals that the anti-Stokes radiation is emitted into a cone whose axis is parallel to the beam-propagation direction (Fig. 3.11). The apex angle β of this cone is obtained by multiplying (3.35) with $\boldsymbol{k}_a$

$$2\boldsymbol{k}_L \cdot \boldsymbol{k}_a = 2k_L k_a \cos\beta = \boldsymbol{k}_S \cdot k_a \cos\alpha + k_a^2 . \tag{3.36a}$$

With $k = n \cdot \omega / c$ this can be written as

$$\cos\beta = \frac{n(\omega_S)\omega_S \cos\alpha + n(\omega_a)\omega_a}{2n(\omega_L)\omega_L} . \tag{3.36b}$$

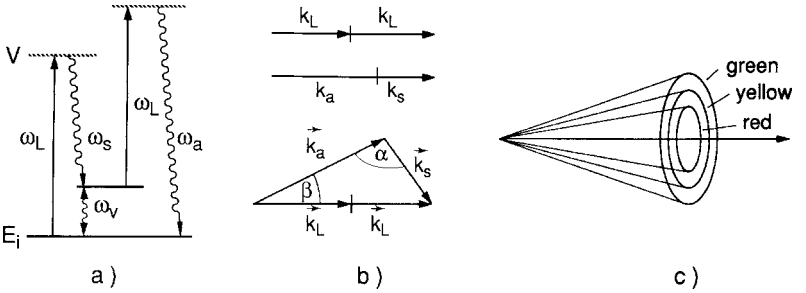

Fig. 3.11a–c. Generation of stimulated anti-Stokes radiation: (**a**) term diagram illustrating energy conservation; (**b**) vector diagram of momentum conservation for the collinear and noncollinear case; (**c**) radiation cone for different values of $\boldsymbol{k}_S$ showing red, yellow, and green rings of anti-Stokes radiation excited by a ruby laser at 694 nm

For $n(\omega_S) = n(\omega_a) = n(\omega_L)$ the collinear case can be realized ($\alpha = \beta = 0$). This is exactly what has been observed [3.39, 3.42].

Let us briefly summarized the differences between the linear (spontaneous) and the nonlinear (induced) Raman effect:

- While the intensity of spontaneous Raman lines is proportional to the incident pump intensity, but lower by several orders of magnitude compared with the pump intensity, the stimulated Stokes or anti-Stokes radiation depend in a nonlinear way on I_p but have intensities comparable to that of the pump wave.
- The stimulated Raman effect is observed only above a threshold pump intensity, which depends on the gain of the Raman medium and the length of the pump region.
- Most Raman-active substances show only one or two Stokes lines at the frequencies $\omega_S = \omega_L - \omega_V$ in stimulated emission. At higher pump intensities, however, lines at the frequencies $\omega = \omega_L - n\omega_V$ ($n = 1, 2, 3$), which do not correspond to overtones of vibrational frequencies, have been observed besides these Stokes lines. Because of the anharmonicity of molecular vibrations, the vibrational levels in an unharmonic potential have energies $E_v = \hbar\omega_v(n + \frac{1}{2}) - x_k\hbar(n + \frac{1}{2})^2$ and therefore the spontaneous Raman lines from vibrational overtones are shifted against ω_L by $\Delta\omega = n\omega_v - (n^2 + n)x_k$, where x_k represent the anharmonicity constants. In Fig. 3.12 is illustrated that these higher-order Stokes lines are generated by consecutive Raman processes, induced by the pump wave, the Stokes wave, etc.
- The linewidths of spontaneous and stimulated Raman lines depend on the linewidth of the pump laser. For narrow linewidths, however, the width of the stimulated Raman lines becomes smaller than that of the spontaneous lines, which are Doppler-broadened by the thermal motion of the scattering molecules. A Stokes photon $\hbar\omega_S$, which is scattered into an angle ϕ against the incident laser beam by a molecule moving with the velocity $\boldsymbol{v}$,

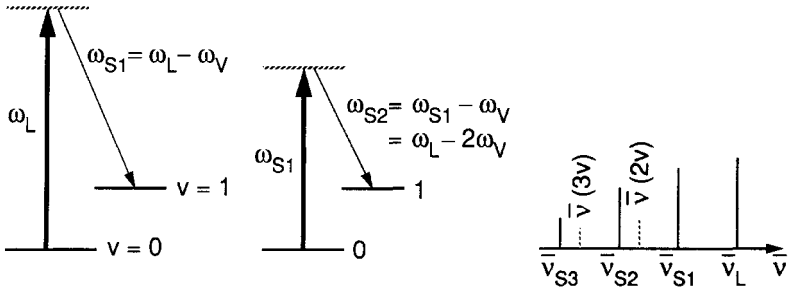

Fig. 3.12. Level diagram for the generation of higher-order Stokes sidebands, which differ from the vibrational overtone frequencies

has a Doppler-shifted frequency

$$\begin{aligned}\omega_s &= \omega_L - \omega_V - (\boldsymbol{k}_L - \boldsymbol{k}_S)\cdot\boldsymbol{v} \\ &= \omega_L - \omega_v - [1 - (k_S/k_L)\cos\phi]\boldsymbol{k}_L\cdot\boldsymbol{v}\,.\end{aligned} \tag{3.37}$$

In the case of spontaneous Raman scattering we have $0 \leq \phi \leq 2\pi$, and the spontaneous Raman lines show a Doppler width that is $(k_S/k_L) = (\omega_S/\omega_L)$ times that of fluorescence lines at ω_L. For induced Raman scattering $\boldsymbol{k}_S \parallel \boldsymbol{k}_L \rightarrow \cos\phi = 1$, and the bracket in (3.37) has the value $(1 - k_S/k_L) \ll 1$, if $\omega_V \ll \omega_L$.

- The main merit of the stimulated Raman effect for molecular spectroscopy may be seen in the much higher intensities of stimulated Raman lines. During the same measuring time one therefore achieves a much better signal-to-noise ratio than in linear Raman spectroscopy. The experimental realization of stimulated Raman spectroscopy is based on two different techniques:

(a) Stimulated Raman gain spectroscopy (SRGS), where a strong pump laser at ω_L is used to produce sufficient gain for the Stokes radiation at ω_S according to (3.31). This gain can be measured with a weak tunable probe laser tuned to the Stokes wavelengths [3.43] (Fig. 3.13).
(b) Inverse Raman spectroscopy (IRS), where the attenuation of the weak probe laser at ω_1 is measured when the strong pump laser at ω_2 is tuned through Stokes or anti-Stokes transitions [3.44].

Several high-resolution stimulated Raman spectrometers have been built [3.43–3.45] that are used for measurements of linewidths and Raman line positions in order to gain information on molecular structure and dynamics. A good compromise for obtaining a high resolution and a large signal-to-noise ratio is to use a pulsed pump laser and a single-mode cw probe laser (quasi-cw spectrometer [3.45]). The narrow-band pulsed laser can be realized by pulsed amplification of a single-mode cw laser (Vol. 1, Sect. 5.7). For illustration Fig. 3.13 shows a typical quasi-cw stimulated Raman spectrometer,

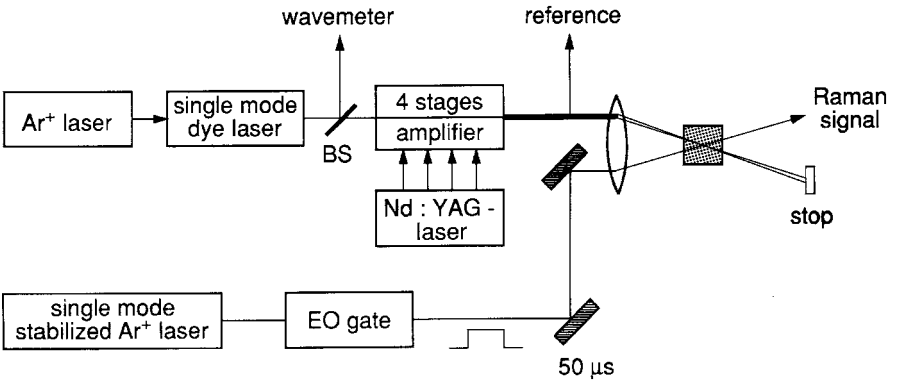

Fig. 3.13. Schematic diagram of a stimulated Raman spectrometer with pulsed, amplified cw pump laser and a single-mode cw probe laser [3.47]

where the wavelengths of the tunable dye laser are measured with a traveling Michelson wavemeter (Vol. 1, Sect. 4.4)

There is another important application of stimulated Raman scattering in the field of *Raman lasers*. With a tunable pump laser at the frequency ω_L, intense coherent radiation sources at frequencies $\omega_L \pm n\omega_V$ $(n = 1, 2, 3, \ldots)$ can be realized that cover the UV and infrared spectral range if visible pump lasers are used (Vol. 1, Sect. 5.8).

More details on the stimulated Raman effect and reference to experiments in this field can be found in [3.11, 3.46–3.52].

3.3.2 Coherent Anti-Stokes Raman Spectroscopy

In Sect. 3.3.1 we discussed the observation that a sufficiently strong incident pump wave at the frequency ω_L can generate an intense Stokes wave at $\omega_S = \omega_L - \omega_V$. Under the combined action of both waves, the nonlinear polarization P_{NL} of the medium is generated that contains contributions at the frequencies $\omega_V = \omega_L - \omega_S$, $\omega_S = \omega_L - \omega_V$, and $\omega_a = \omega_L + \omega_V$. These contributions act as driving forces for the generation of new waves. Provided that the phase-matching conditions $2\boldsymbol{k}_L = \boldsymbol{k}_S + \boldsymbol{k}_a$ can be satisfied, a strong anti-Stokes wave $E_a \cos(\omega_a t - \boldsymbol{k}_a \cdot \boldsymbol{r})$ is observed in the direction of $\boldsymbol{k}_a$.

Despite the enormous intensities of stimulated Stokes and anti-Stokes waves, stimulated Raman spectroscopy has been of little use in molecular spectroscopy. The high threshold, which, according to (3.30), depends on the molecular density N, the incident intensity $I \propto E_L^2$, and the square of the small polarizability term $(\partial\alpha_{ij}/\partial q)$ in (3.27), limits stimulated emission to only the strongest Raman lines in materials of high densities N.

The recently developed technique of coherent anti-Stokes Raman spectroscopy (CARS), however, combines the advantages of signal strength obtained in stimulated Raman spectroscopy with the general applicability of

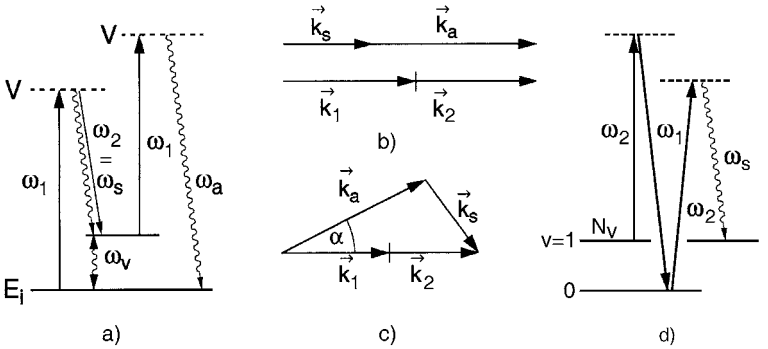

Fig. 3.14. (**a**) Level diagram of CARS; (**b**) vector diagrams for phase matching in gases with negligible dispersion and (**c**) in liquids or solids with noticeable dispersion; (**d**) generation of coherent Stokes radiation at $\omega_S = 2\omega_2 - \omega_1$

spontaneous Raman spectroscopy [3.46–3.57]. In this technique *two* lasers are needed. The frequencies ω_1 and ω_2 of the two incident laser waves are chosen such that their difference $\omega_1 - \omega_2 = \omega_V$ coincides with a Raman-active vibration of the molecules under investigation. These two incident waves correspond to the pump wave ($\omega_1 = \omega_L$) and the Stokes wave ($\omega_2 = \omega_S$) in stimulated Raman scattering. The advantage is that the Stokes wave at ω_2 is already present and does not need to be generated in the medium. These two waves are considered in (3.19).

Because of the nonlinear interaction discussed in Sect. 3.3.1, new Stokes and anti-Stokes waves are generated (Fig. 3.14d). The waves ω_1 and ω_2 produce a large population density of vibrationally excited molecules by stimulated Raman scattering. These excited molecules act as the nonlinear medium for the generation of anti-Stokes radiation at $\omega_a = 2\omega_1 - \omega_2$ by the incident wave with frequency ω_1. In a similar way, a Stokes wave with frequency $\omega_s = 2\omega_2 - \omega_1$ is generated by the incident waves at ω_1 and ω_2 (Fig. 3.14d). Since four waves are involved in the generation of the anti-Stokes wave, CARS is called a *four-wave parametric mixing process* (Fig. 3.15).

It can be derived from (3.33) that the power S of the CARS signal (which is proportional to the square of the amplitude E_a)

$$S \propto N^2 I_1^2 I_2 \,, \tag{3.38}$$

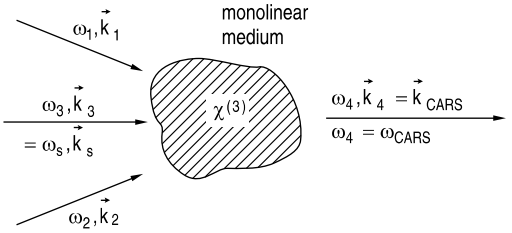

Fig. 3.15. CARS as a four-wave mixing process

increases with the square N^2 of the molecular density N and is proportional to the product $I_1(\omega_1)^2 I_2(\omega_2)$ of the pump laser intensities. It is therefore necessary to use either high densities N or large intensities I. If the two pump beams are focused into the sample, most of the CARS signal is generated within the local volume where the intensities are maximum. CARS spectroscopy therefore offers high spatial resolution.

If the incident waves are at *optical* frequencies, the difference frequency $\omega_R = \omega_1 - \omega_2$ is small compared with ω_1 in the case of rotational–vibrational frequencies ω_R. In gaseous Raman samples the dispersion is generally negligible over small ranges $\Delta\omega = \omega_1 - \omega_2$ and satisfactory phase matching is obtained for *collinear* beams. The Stokes wave at $\omega_S = 2\omega_2 - \omega_1$ and the anti-Stokes wave at $\omega_a = 2\omega_1 - \omega_2$ are then generated in the same direction as the incoming beams (Fig. 3.14b). In liquids, dispersion effects are more severe and the phase-matching condition can be satisfied over a sufficiently long coherence length only, if the two incoming beams are crossed at the phase-matching angle (Fig. 3.14c).

In the collinear arrangement the anti-Stokes wave at $\omega_a = 2\omega_1 - \omega_2$ ($\omega_a > \omega_1$!) is detected through filters that reject both incident laser beams as well as the fluorescence that may be generated in the sample. Figure 3.16 illustrates an early experimental setup used for rotational–vibrational spectroscopy of gases by CARS [3.58]. The two incident laser beams are provided by a Q-switched ruby laser and a tunable dye laser that was pumped by this ruby laser. Because the gain of the anti-Stokes wave depends quadratically on the molecular density N (see (3.38)), megawatt-range power levels of the incident beams are required for gaseous samples, while kilowatt powers are sufficient for liquid samples [3.59].

The most common pump system for pulsed CARS experiments are two dye lasers pumped by the same pump laser (N_2 laser, excimer laser, or frequency-doubled Nd:YAG laser). This system is very flexible because both frequencies ω_1 and ω_2 can be varied over large spectral ranges. Since both the frequency and intensity fluctuations of the dye lasers result in strong intensity

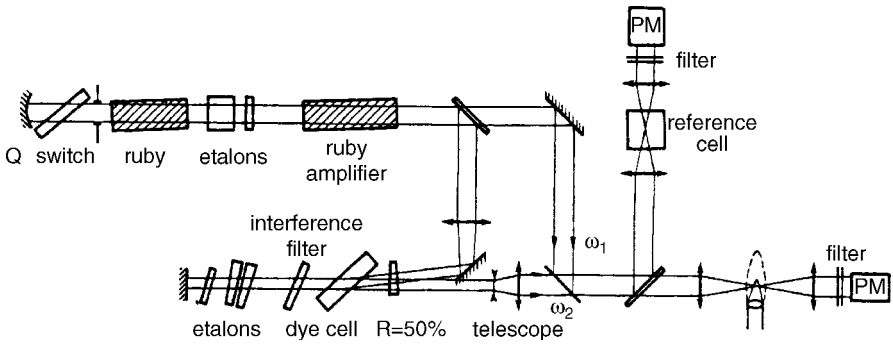

Fig. 3.16. Experimental setup of an early CARS experiment in gases using a ruby laser and a dye laser pumped by the ruby laser [3.58]

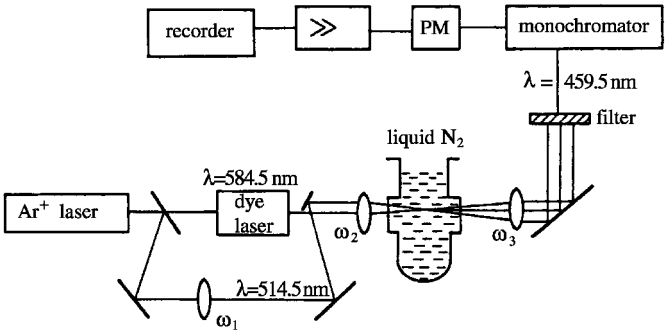

Fig. 3.17. Experimental setup for cw CARS in liquids [3.59]

fluctuations of the CARS signal, the stability of the dye lasers needs particular attention. With compact and stable systems the signal fluctuations can be reduced below 10% [3.60].

In addition, many CARS experiments have been performed with cw dye lasers with liquid samples as well as with gaseous ones. An experimental setup for cw CARS of liquid nitrogen is shown in Fig. 3.17, where the two incident collinear pump waves are provided by the 514.5-nm argon laser line (ω_1) and a cw dye laser (ω_2) pumped by the same argon laser [3.59].

The advantage of cw CARS is its higher spectral resolution because the bandwidth $\Delta\nu$ of single-mode cw lasers is several orders of magnitude below that of pulsed lasers. In order to obtain sufficiently high intensities, intracavity excitation has been used. A possible experimental realization (Fig. 3.18) places the sample cell inside the ring resonator of an argon ion laser, where the cw dye laser is coupled into the resonator by means of a prism [3.44].

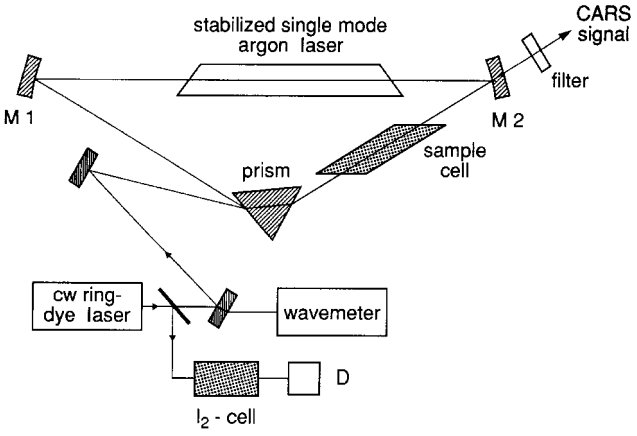

Fig. 3.18. Schematic arrangement of a cw CARS spectrometer with intracavity excitation of the sample [3.44]

The CARS signal generated in the sample cell at the beam waist of the resonator is transmitted through the dichroic mirror M2 and is spectrally purified by a filter or a prism and a monochromator before it reaches a photomultiplier.

High-resolution CARS can be also performed with injection-seeded pulsed dye lasers [3.44, 3.61]. If the radiation of a single-mode cw dye laser with frequency ω is injected into the cavity of a pulsed dye laser that has been mode matched to the Gaussian beam of the cw laser (Vol. 1, Sect. 5.8), the amplification of the gain medium is enhanced considerably at the frequency ω and the pulsed laser oscillates on a single cavity mode at the frequency ω. Only some milliwatts of the cw laser are needed for injection, while the output of the single-mode pulsed laser reaches several kilowatts, which may be further amplified (Vol. 1, Sect. 5.5). Its bandwidth $\Delta\nu$ for pulses of duration Δt is only limited by the Fourier limit $\Delta\nu = 1/(2\pi\Delta t)$.

3.3.3 Resonant CARS and BOX CARS

If the frequencies ω_1 and ω_2 of the two incident laser waves are chosen to match a molecular transition, one or even two of the virtual levels in Fig. 3.14 coincide with a real molecular level. In this case of *resonant CARS*, the sensitivity may be increased by several orders of magnitude. Because of the larger absorption of the incident waves, the absorption path length must be sufficiently short or the density of absorbing molecules must be correspondingly small [3.62, 3.63].

A certain disadvantage of collinear CARS in gases is the spatial overlap of the two parallel incident beams with the signal beam. This overlap must be separated by spectral filters. This disadvantage can be overcome by the BOX CARS technique [3.64], where the pump beam of laser L1 ($\boldsymbol{k}_1, \omega_1$) is split into two parallel beams that are focused by a lens into the sample (Fig. 3.19b), where the directions of the three incoming beams match the vector diagram of Fig. 3.19a. The CARS signal beam can now be separated by geometrical means (beam stop and apertures). For comparison the vector diagrams of the phase-matching condition (3.35) are shown in Fig. 3.20 for the general case ($\boldsymbol{k}_1 \neq \boldsymbol{k}_2$), the collinear CARS arrangement, and for BOX CARS, where the vector diagram has the form of a box. From Fig. 3.19a with the relation $|\boldsymbol{k}| = n \cdot \omega/c$, the phase-matching conditions

$$\begin{aligned} n_2\omega_2 \sin\theta &= n_3\omega_3 \sin\varphi \,, \\ n_2\omega_2 \cos\theta + n_3\omega_3 \cos\varphi &= 2n_1\omega_1 \cos\alpha \,, \end{aligned} \tag{3.39}$$

can be derived, which yield for $\theta = \alpha$ the relation

$$\sin\varphi = \frac{n_2\omega_2}{n_3\omega_3} \sin\alpha \,, \tag{3.40}$$

between the angle φ of the CARS signal beam $\boldsymbol{k}_\mathrm{a} = \boldsymbol{k}_3$ against the z-direction and the angle α of the incident beams.

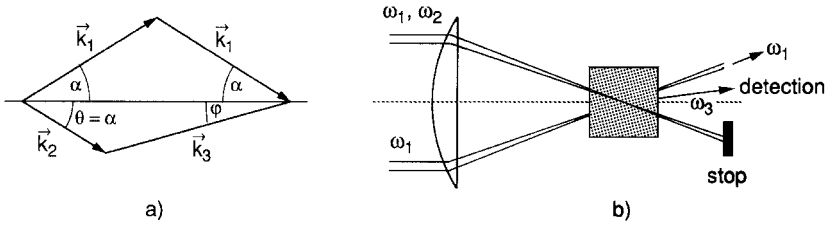

Fig. 3.19a,b. Wave vector diagram for BOX CARS (**a**) and experimental realization (**b**)

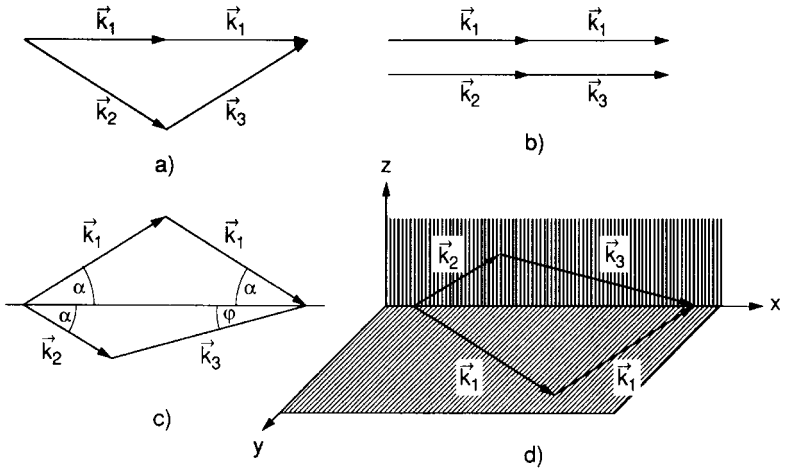

Fig. 3.20a–d. Comparison of phase-matching diagrams for CARS: (**a**) for the general case $\boldsymbol{k}_1 \nparallel \boldsymbol{k}_2$; (**b**) the collinear case $\boldsymbol{k}_1 \parallel \boldsymbol{k}_2$; (**c**) for BOX CARS; and (**d**) for folded BOX CARS

The CARS signal is generated within the common overlap volume of the three incident beams. This BOX-CAR technique considerably increases the spatial resolution, which may reach values below 1 mm.

In another beam configuration (folded BOX CARS), the pump beam with ω_2 is split into two parallel beams, which are directed by the focusing lens in such a way that the wave vectors $\boldsymbol{k}_2$ and $\boldsymbol{k}_3 = \boldsymbol{k}_{as}$ are contained in a plane orthogonal to that of the two $\boldsymbol{k}_1$ vectors (Fig. 3.20d). This has the advantage that neither of the two pump beams overlaps the signal beam at the detector [3.65]. If the Raman shifts are small, spectral filtering becomes difficult and the advantage of this folded BOX CAR technique is obvious.

The advantages of CARS may be summarized as follows:

- The signal levels in CARS may exceed those obtained in spontaneous Raman spectroscopy by a factor of $10^4 - 10^5$.
- The higher frequency $\omega_3 > \omega_1$, ω_2 of the anti-Stokes waves allows one to use filters that reject the incident light as well as fluorescence light.
- The small beam divergence allows one to place the detector far away from the sample, which yields excellent spatial discrimination against

fluorescence or thermal luminous background such as occurs in flames, discharges, or chemiluminescent samples.

- The main contribution to the anti-Stokes generation comes from a small volume around the focus of the two incident beams. Therefore very small sample quantities (microliters for liquid samples or millibar pressures for gaseous samples) are required. Furthermore, a high spatial resolution is possible, which allows one to probe the spatial distribution of molecules in definite rotational–vibrational levels. The measurements of local temperature variations in flames from the intensity of anti-Stokes lines in CARS is an example where this advantage is utilized.
- The high spatial resolution is utilized in CARS microscopy, which is mainly applied to the investigation of biological cells and their compositions (see Sect. 3.4.3).
- A high spectral resolution can be achieved without using a monochromator. The Doppler width $\Delta\omega_D$, which represents a principal limitation in 90° spontaneous Raman scattering, is reduced to $[(\omega_2-\omega_1)/\omega_1]\Delta\omega_D$ for the collinear arrangement used in CARS. While a resolution of 0.3 to $0.03\,\mathrm{cm}^{-1}$ is readily obtained in CARS with pulsed lasers, even linewidths down to $0.001\,\mathrm{cm}^{-1}$ have been achieved with single-mode lasers.

The main disadvantages of CARS are the expensive equipment and strong fluctuations of the signals caused by instabilities of intensities and alignments of the incident laser beams. The sensitivity of detecting low relative concentrations of specified sample molecules is mainly limited by interference with the nonresonant background from the other molecules in the sample. This limitation can be overcome, however, by resonant CARS.

3.3.4 Hyper-Raman Effect

The higher-order terms $\beta\boldsymbol{EE}$, $\gamma\boldsymbol{EEE}$ in the expansion (3.18a) of $\boldsymbol{p}(E)$ represent the hyper-Raman effect. Analogous to (3.3), we can expand β in a Taylor series in the normal coordinates $q_n = q_{n0}\cos(\omega_n t)$

$$\beta = \beta_0 + \sum_{n=1}^{2Q}\left(\frac{\partial\beta}{\partial q_n}\right)_0 q_n + \ldots \,. \tag{3.41}$$

Assume that two laser waves $E_1 = E_{01}\cos(\omega_1 t - k_1 z)$ and $E_2 = E_{02}\cos(\omega_2 t - k_2 t)$ are incident on the Raman sample. From the third term in (3.18a) we then obtain with (3.41) contributions to $p(E)$ due to β_0

$$\beta_0 E_{01}^2\cos(2\omega_1 t)\,, \quad \text{and} \quad \beta_0 E_{02}^2\cos(2\omega_2 t)\,, \tag{3.42}$$

which give rise to *hyper-Rayleigh scattering* at frequencies $2\omega_1$, $2\omega_2$ and $\omega_1+\omega_2$ (Fig. 3.21a). The term $(\partial\beta/\partial q_n)q_{n0}\cos(\omega_n t)$ of (3.41) inserted into (3.18a) yields contributions

$$p^{\mathrm{HR}} \propto \left(\frac{\partial\beta}{\partial q}\right)_0 q_{n0}[\cos(2\omega_1 \pm \omega_n)t + \cos(2\omega_2 \pm \omega_n)t]\,, \tag{3.43}$$

which are responsible for *hyper-Raman scattering* (Fig. 3.21b,c) [3.66].

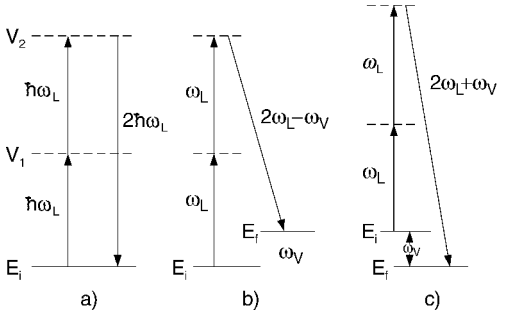

Fig. 3.21a–c. Hyper-Rayleigh scattering (**a**), Stokes hyper-Raman (**b**), and anti-Stokes hyper-Raman scattering (**c**)

Since the coefficients $(\partial\beta/\partial q)_0$ are very small, one needs large incident intensities to observe hyper-Raman scattering. Similar to second-harmonic generation (Vol. 1, Sect. 5.8), hyper-Rayleigh scattering is forbidden for molecules with a center of inversion. The hyper-Raman effect obeys selection rules that differ from those of the linear Raman effect. It is therefore very attractive to molecular spectroscopists since molecular vibrations can be observed in the hyper-Raman spectrum that are forbidden for infrared as well as for linear Raman transitions. For example, spherical molecules such as CH_4 have no pure rotational Raman spectrum but a hyper-Raman spectrum, which was found by Maker [3.67]. A general theory for rotational and rotational–vibrational hyper-Raman scattering has been worked out by Altmann and Strey [3.68].

The intensity of hyper-Raman lines can be considerably enhanced when the molecules under investigation are adsorbed at a surface [3.69], because the surface lowers the symmetry and increases the induced dipole moments.

Similar to the induced Raman effect, the hyper-Raman effect can also be used to generate coherent radiation in spectral ranges where no intense lasers exist. One example is the generation of tunable radiation around 16 μm by the stimulated hyper-Raman effect in strontium vapor [3.70].

3.3.5 Summary of Nonlinear Raman Spectroscopy

In the previous subsections we briefly introduced some nonlinear techniques of Raman spectroscopy. Besides stimulated Raman spectroscopy, Raman gain spectroscopy, inverse Raman spectroscopy, and CARS, several other special techniques such as the Raman-induced Kerr effect [3.71] or coherent Raman ellipsometry [3.72] also offer attractive alternatives to conventional Raman spectroscopy.

All these nonlinear techniques represent coherent third-order processes analogous to saturation spectroscopy, polarization spectroscopy, or two-photon absorption (Chap. 2), because the magnitude of the nonlinear signal is proportional to the third power of the involved field amplitudes (3.18).